ELSEVIER

Physica D 103 (1997) 273–293

PHYSICA D

Collective chaos and noise in the globally coupled complex Ginzburg–Landau equation

Marie-Line Chabanol [a,*], Vincent Hakim [a], Wouter-Jan Rappel [b]

[a] *Laboratoire de Physique Statistique, 24 rue Lhomond, 75231 Paris Cedex 05, France*

[b] *Northeastern University, Department of Physics, Boston, MA 02116, USA*

Abstract

We study a globally coupled version of the complex Ginzburg–Landau equation (GC-CGLE) which consists of a large number N of identical two-dimensional oscillators coupled through their mean amplitude. Depending on parameter values, different dynamical regimes are attained. We focus particularly on an interesting regime where the individual oscillators follow erratic motion but in a sufficiently coherent way so that the average motion does not vanish when N becomes large and is also chaotic. A simple description of this state is proposed by considering the motion of a single forced two-dimensional system which has both a limit cycle and a fixed point as stable attractors. Determining which of these two deterministic attractors is selected by a weak noise and how this depends on the parameter of the reduced system allows us to determine self-consistently the average amplitude and dominant frequency of the collective behaviour of the full system. Finally, we show that adding a small noise to the GC-CGLE transforms the chaotic collective behaviour into a purely periodic one.

1. Introduction

Several problems of physics and biology can be described by the dynamics of a network of coupled oscillators [1–6]. An interesting class of such systems is formed by globally coupled arrays where each oscillator is coupled to all the other ones in an identical way. We focus here on a globally coupled version of the complex Ginzburg–Landau equation (GC-CGLE) which has been introduced previously [7,8],

$$\partial_t A_j = (1 + \mathrm{i}\eta)(\overline{A} - A_j) + \mu A_j - (1 + \mathrm{i}\alpha)|A_j|^2 A_j, \quad j = 1, \ldots, N. \tag{1}$$

This is an array of N two-dimensional limit cycle oscillators (described by the complex numbers A_j) globally coupled through their average amplitude $\overline{A}$:

$$\overline{A} = \frac{1}{N}\sum_{k=1}^{N} A_k. \tag{2}$$

* Corresponding author.

PII S0167-2789(96)00263-1

Depending on the value of the parameters α, η and μ, this system exhibits several different regimes which are typical of what is observed in globally coupled arrays. The different possibilities and their location in parameter space are recalled in the next section following results obtained previously. We focus more specifically on a complex and particularly interesting regime where individual oscillators follow erratic motions but in a sufficiently coherent way so that the average $\overline{A}$ does not tend to zero when N becomes large . In this regime, $\overline{A}(t)$ has a chaotic motion, peaked around a dominant frequency. A simple approach enables us to understand qualitatively some salient features of this state (particularly the distribution of the A_j in the complex plane) and to compute quantitatively some of its properties (average amplitude and dominant frequency of $\overline{A}(t)$). It consists in analysing the motion of a single forced two-dimensional system, the forcing of which is to be determined self-consistently. In the parameter region of interest this deterministic system has two stable attractors, a fixed point and a limit cycle. This leads to a one-parameter family of self-consistent solutions, the parameter being the proportion of oscillators on one of the attractors. In order to choose one particular solution out of this continuum family, we are led to consider how adding a weak noise selects one of the deterministic attractors of our reduced two-dimensional system, an interesting problem in its own right in this out-of-equilibrium non-hamiltonian context [9–12]. We finally investigate the sensitivity of this chaotic collective regime to the addition of external noise on the elements of the globally coupled array [13]. We show that the addition of a weak external noise transforms the chaotic behaviour of $\overline{A}(t)$ into a purely periodic one without drastically altering most other qualitative features. On the contrary, a first-order transition to a periodic state with $\overline{A}(t) = 0$ is obtained for a larger noise amplitude. Technical details of some calculations are presented in Appendices A and B.

2. Dynamical regimes of the GC-CGLE

Eq. (1) has been integrated numerically in [7,8]. We have done it by using a second-order Runge–Kutta algorithm with a time step generally taken to be $dt = 0.01$ but sometimes reduced to check that our results were not affected by the discretization. Arrays from $N = 50$ up to $N = 10000$ sites were used but in general reliable results are already obtained with the smaller arrays.

Four qualitatively different regimes have been observed. Their location is shown in Fig. 1 in the (η, μ) parameter space with a fixed $\alpha = 2$. Other cuts in the 3-parameter space are presented in [7,8].

The dynamics in region I is the simplest. All the oscillators follow identical trajectories (i.e. $A_j(t) = \overline{A(t)}$ for all j). Therefore, the coupling term in Eq. (1) vanishes and the oscillators follow the limit cycle of the uncoupled system

$$A(t) = \sqrt{\mu}\exp(-i\alpha\mu t). \tag{3}$$

Region II is equally simple. All the oscillators are rotating at the same constant angular velocity on a circle of radius $\sqrt{\mu - 1}$ centred at the origin, with their phases adjusted so that $\overline{A(t)} = 0$,

$$A_j = \sqrt{\mu - 1}\,\exp(i[(\alpha - \eta - \alpha\mu)t + \phi_j]) \tag{4}$$

with

$$\frac{1}{N}\sum_{j=1}^{N}\exp(i\phi_j) = 0. \tag{5}$$

There are of course many different ways to realize condition (5).

The regimes of regions I and II are rather simple and their stability boundaries can be obtained analytically without difficulty (see Appendix A for details). For region I, one obtains one zero eigenvalue coming from the invariance

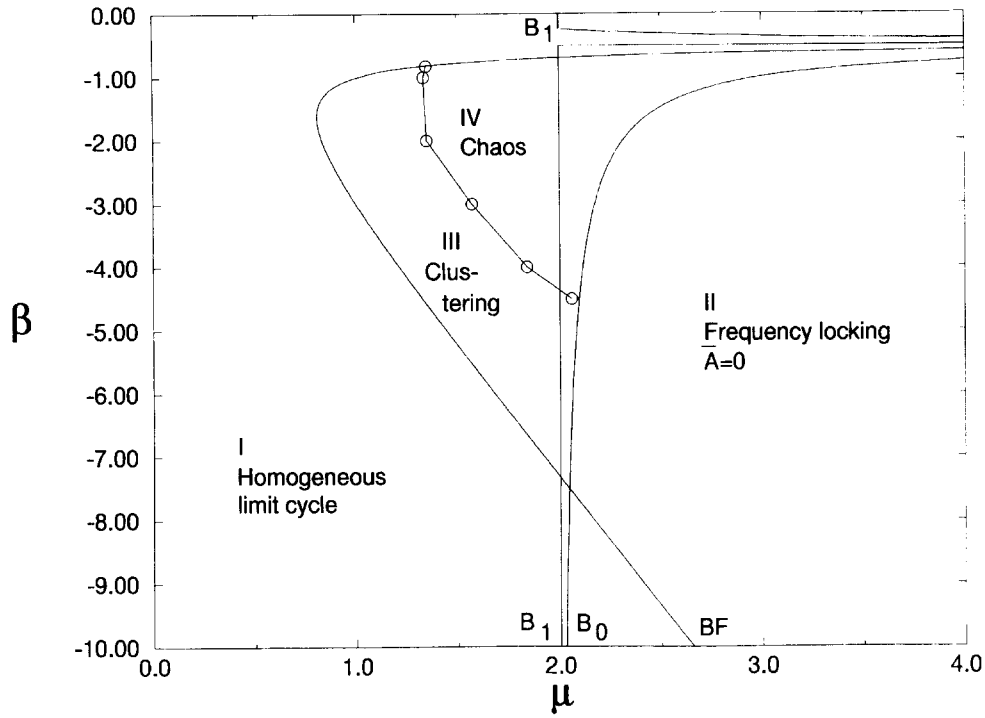

Fig. 1. Phase diagram for $\alpha = 2$.

of Eq. (1) under a global phase change, one negative eigenvalue -2μ and $N-1$ sets of two eigenvalues λ_1 and λ_2, solutions of the real second-order equation

$$\lambda^2 + 2(\mu+1)\lambda + 2\mu(1+\alpha\eta) + 1 + \eta^2 = 0. \tag{6}$$

The condition of stability of the homogeneous limit cycle (which generalizes the well-known Benjamin–Feir stability criterion for the continuous complex Ginzburg–Landau equation [14]) is therefore

$$2\mu(1+\alpha\eta) + (1+\eta^2) > 0. \tag{7}$$

Similarly, one can diagonalize the stability matrices for the states of region II. One obtains $(N-2)$ negative eigenvalues equal to $-2(\mu-1)$ and $(N-2)$ zero eigenvalues, reflecting the dimensions of the manifold of locked fixed points (i.e. N arbitrary real phases subject to the condition $\overline{A}=0$ which gives two real constraints). The four remaining eigenvalues depend on the particular locked state under consideration but only through the real parameter $\Delta = |(1/N)\sum_j \exp(2i\phi_j)|$, $0 \le \Delta \le 1$, where ϕ_j denotes the phase of the jth oscillator on the limit cycle. Δ characterizes the repartition of the oscillator phases on the limit cycle. These four eigenvalues are the roots of the degree 4 characteristic polynomial $P_4(\lambda)$ with

$$P_4(\lambda) = P_2(\lambda)P_2^*(\lambda) - \Delta^2(\mu-1)^2(1+\alpha^2)(1+\eta^2), \tag{8}$$

where the degree 2 polynomial $P_2(\lambda)$ is given by

$$P_2(\lambda) = \lambda^2 - \lambda(3 - 2\mu + i\eta) - (\mu-1)(1+i\eta)(1-i\alpha). \tag{9}$$

The stability criterion is simply that all the roots of $P_4(\lambda)$ have a negative real part. For $\Delta = 0$, they coincide with the roots of $P_2(\lambda)$ and $P_2^*(\lambda)$. One obtains

$$\begin{aligned} &2\mu - 3 > 0, \\ &(\mu - 2)\eta^2 - 4\alpha\eta(\mu - 1)(\mu - 2) + \alpha^2(1 - \mu) - (2\mu - 3)^2 > 0. \end{aligned} \tag{10}$$

For an arbitrary Δ, one can use the Routh–Hurwitz criterion [15] which gives

$$\begin{aligned} &2\mu - 3 > 0, \\ &[(2\mu - 3)^2 + \eta^2][(\mu - 2)\eta^2 - 4\alpha\eta(\mu - 1)(\mu - 2) + \alpha^2(1 - \mu) - (2\mu - 3)^2] \\ &\quad + \Delta^2(\mu - 1)(2\mu - 3)^2(1 + \alpha^2)(1 + \eta^2) > 0. \end{aligned} \tag{11}$$

The stability limit of the state with phases uniformly distributed on the limit circle is the line B_0 in Fig. 1. States with phases distributed unevenly on the limit circle have actually a slightly wider range of stability. The configuration of this type which has the larger domain of stability is formed by two populations of oscillators, having opposite phases. The boundary of stability of this last configuration is denoted B_1 in Fig. 1. However, in the parameter region between the line B_0 and B_1, these nonuniform states appear to have a small basin of attraction and some care has to be exercised in choosing the initial condition if one wants to observe them. Otherwise, the chaotic state of region IV (described below) is reached most of the time.

In region III, the system exhibits clustering. Namely, it breaks down into a small number (2 or 3) of groups of oscillators in identical states. The dynamics effectively reduces to that of a low number of coupled oscillators (with different weights) and can be periodic, quasiperiodic or even chaotic [8]. For given parameters (α, η, μ), the number of oscillators in each cluster is not fixed but depends on the initial condition in a way that has not been precisely analysed. Clustering generally appears in globally coupled systems and was for example described in [2] for coupled maps and in [6] for phase models.

The dynamical behaviour in region IV is the most complex and will be the focus of the next sections. The magnitude of $\overline{A(t)}$ remains of order 1 as the number of oscillators increases (see Fig. 2) but the collective dynamics is chaotic. As shown in Fig. 3, the power spectrum of the real part of $\overline{A(t)}$ is peaked around a definite frequency but is broadband.

Moreover, the largest Lyapunov exponent has been computed and found to be positive [7,16]. One interesting feature of this state is that the repartition of the oscillators in the complex plane at a given time is much less disordered than could have been expected. This is quite striking for the parameters of Fig. 4. At a given time all the oscillators stand on a fairly well-defined curve which has roughly the form of an inverted ρ. The whole shape rotates and deforms in time, particularly in the tail part. The motion of individual oscillators alternate between rotations around the loop of the ρ and excursions in the tail part. Understanding this qualitative aspect of the motion as well as determining quantitatively some of its features (mean amplitude of $\overline{A(t)}$, peak frequency in its power spectrum) are the subject of the next section. Before coming to it, we would like to comment shortly on a problem which has been encountered in trying to characterize the collective dynamics of this chaotic state and which is still in need of a good solution.

It concerns the interesting question of determining whether the collective motion is of low dimensionality in the thermodynamic limit ($N \to \infty$). The number of positive Lyapunov exponents for the whole system of N oscillators has been computed using standard techniques and has been found to increase roughly linearly with N [7,16]. This, however, does not say anything about the dimension of the motion of $\overline{A(t)}$ in the thermodynamic limit. For any finite N, one can in principle reconstruct the dynamics of the full system from the time series of $\overline{A(t)}$ using time-delays [17]. This is no longer true in the thermodynamic limit and the possibility exists that the motion of $\overline{A(t)}$ is of strictly lower dimensionality than that of the full system. A simple example of this kind can be obtained by considering an

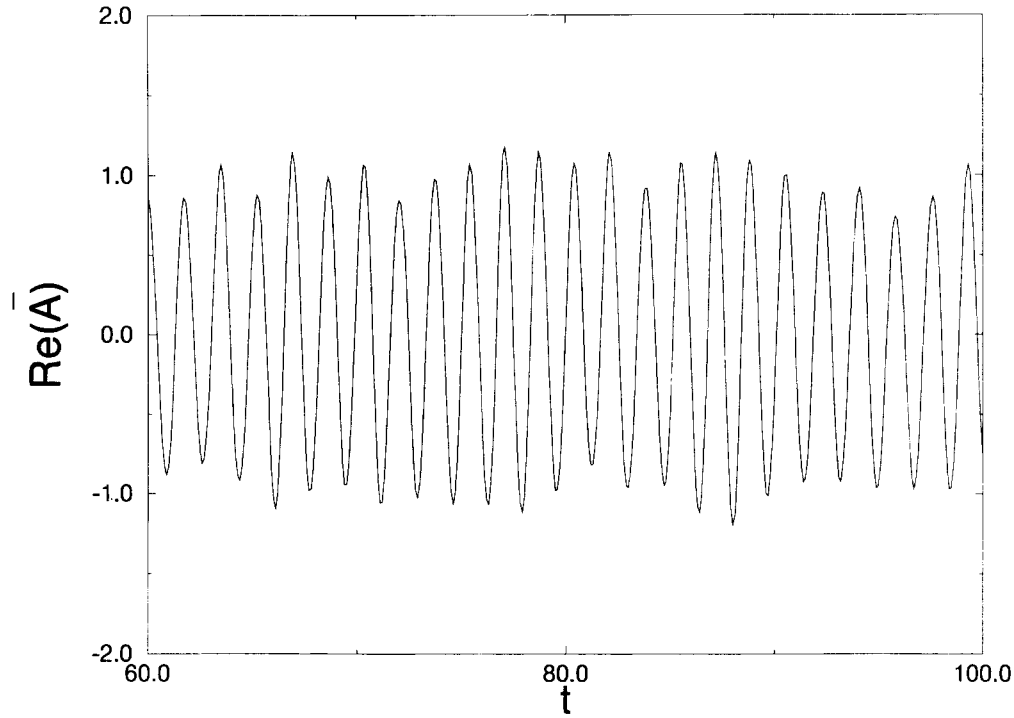

Fig. 2. Time series of the real part of $\overline{A}$. The parameters are $\mu = 2.2, \alpha = 2, \eta = -2$. The number of oscillators is $N = 250$.

ensemble of N identical uncoupled and uncorrelated chaotic motions $x_1(t), \ldots, x_N(t)$ of finite dimension (say 3 for definiteness) and an average zero. Suppose that $A_j(t) = x_1(t) + x_j(t)$ so that

$$\overline{A(t)} = x_1(t) + 1/N \sum_{k=1}^{N} x_k(t). \tag{12}$$

For any finite N, the time series of $\overline{A(t)}$ allows one to reconstruct the full $3N$-dimensional dynamics. However, the sum in (12) has an amplitude of order $1/\sqrt{N}$. It disappears in the thermodynamic limit where the motion of $\overline{A(t)}$ is simply of dimension 3 (instead of $3N$). In our case, the determination of the dimension d_c of the collective motion in the thermodynamic limit has been attempted in two ways. In [7], the method of Grassberger and Procaccia was applied directly to the time series of $\overline{A(t)}$ with the hope of measuring d_c for balls of radius larger than $1/\sqrt{N}$ (or perhaps some other power of $1/N$) and the dimension of the dynamics of the full system for smaller radius. However, the scaling windows turned out to be too small to reach definitive conclusions for the system sizes which were simulated ($50 < N < 5000$). More recently [16], the whole set of Lyapounov has been computed for different system sizes and the different spectra have been compared. The idea was to identify a low-dimensional collective motion in the thermodynamic limit by the fact that some exponents should become independent of N as the system size becomes large. Again, although the results seem to be in favour of a high-dimensional dynamics for $\overline{A(t)}$ no really definitive conclusion has yet been reached.

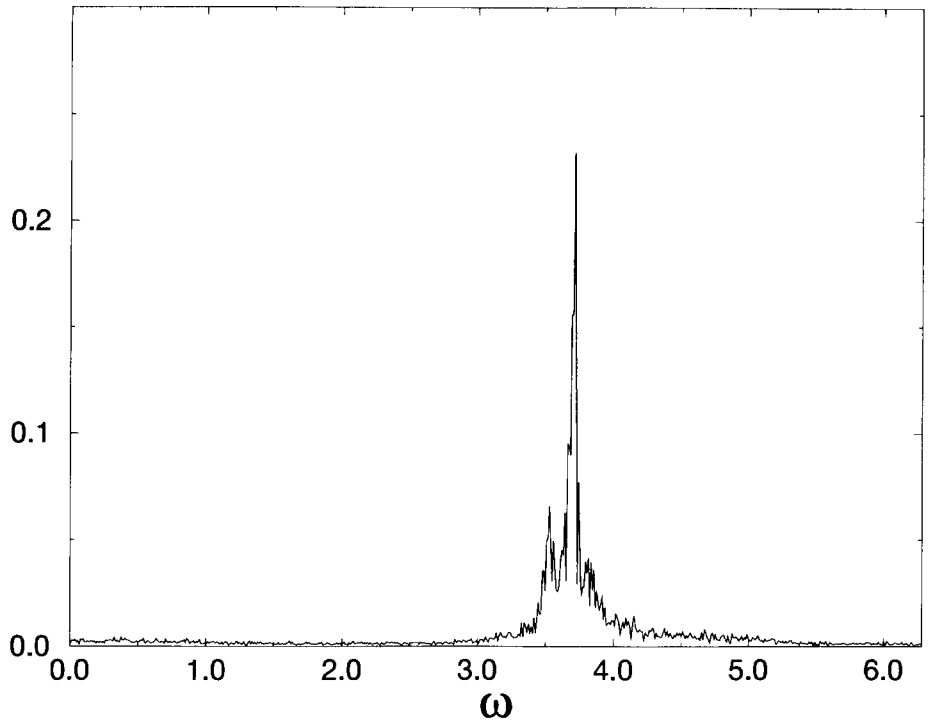

Fig. 3. Power spectrum of Re($\overline{A}(t)$). Parameter values are as in Fig. 2.

3. A simple self-consistent approach to the collective chaotic regime

In this section, a simple approach is developed to obtain some understanding of the complex dynamical regime of region IV. The collective motion has a broad power spectrum but one that is clearly peaked around a dominant frequency. The idea is to first try and understand the origin of this frequency which is neither the frequency of the uncoupled oscillators nor the frequency of the simple periodic regimes of regions I and II (for example for $\alpha = 2, \eta = -2, \mu = 2.2$ the peak is centered around $\omega = -3.7$ whereas, the frequency of the simple periodic regimes would be -4.4 or -0.4). In order to proceed, we will suppose that the collective motion is purely periodic instead of being simply peaked around a dominant frequency so that

$$\overline{A(t)} = R\exp(\mathrm{i}\omega t). \tag{13}$$

This leads us to first consider and compute the characteristics of a general periodic regime. Self-consistency requirements are then shown to lead to a one-parameter family of possible forcings. Finally, compatibility with a weak noise is shown to select a unique self-consistent solution.

3.1. A single oscillator with periodic forcing

The motion of a single oscillator under the periodic forcing (13) is

$$\partial_t A = (1 + \mathrm{i}\eta)R\exp(\mathrm{i}\omega t) + (\mu - 1 - \mathrm{i}\eta)A - (1 + \mathrm{i}\alpha)|A|^2 A. \tag{14}$$

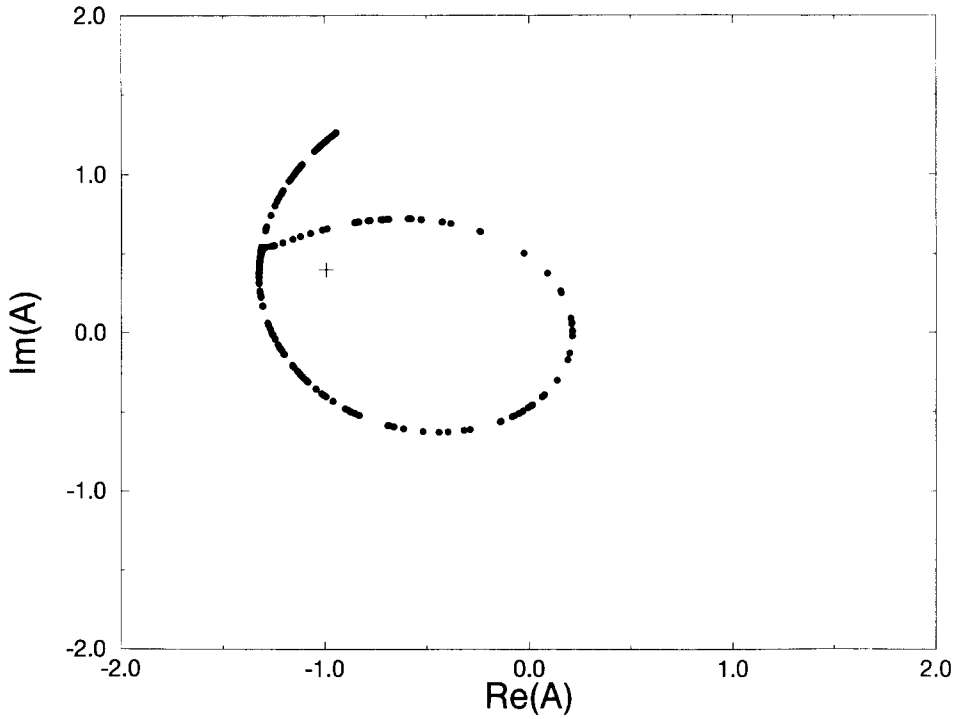

Fig. 4. ρ-shape distribution of oscillators. Parameter values are as in Fig. 2.

It is conveniently studied in a frame rotating at frequency ω where the explicit time dependence disappears. Introducing $B(t) = (\mu - 1)^{-1/2} A(t) \exp[-\mathrm{i}(\omega t + \phi)]$, Eq. (14) becomes simply

$$\partial_\tau B = (1 + \mathrm{i}\Omega)B - (1 + \mathrm{i}\alpha)|B|^2 B + F. \tag{15}$$

A rescaled time $\tau = (\mu - 1)t$ has been introduced and the phase ϕ has been chosen such that $\tan(\phi) = \eta$, $-\frac{1}{2}\pi < \phi < \frac{1}{2}\pi$ so that the two effective parameters Ω and F are real and equal to

$$\Omega = -\frac{\omega + \eta}{\mu - 1}, \qquad F = \frac{\sqrt{1 + \eta^2}}{(\mu - 1)^{3/2}} R. \tag{16}$$

Eq. (15) also appears as an amplitude equation for near resonant forcing of a nonlinear oscillator and it has been studied previously [18]. It has a rich bifurcation set which can be traced back to the existence of a codimension-3 point in the 3-parameter space (Ω, F, α). It is sufficient for our present purpose to consider a cut at fixed $\alpha = 2$ of the general 3-parameter diagram. Fig. 5 shows the main bifurcations in the relevant region of the (Ω, F) parameter space.

In the centre-right region, the phase portrait consists of an attractive limit cycle together with one unstable fixed point in the limit cycle and a pair of fixed points, one stable and one unstable outside the limit cycle (see Fig. 6).

This phase portrait changes in several ways when the parameters Ω and F are varied. When F is decreased one encounters a line of saddle-node bifurcations (noted SN in Fig. 5). The two fixed points outside the limit cycle collide and disappear on SN so that below SN the phase portrait consists of a single limit attractive cycle (together

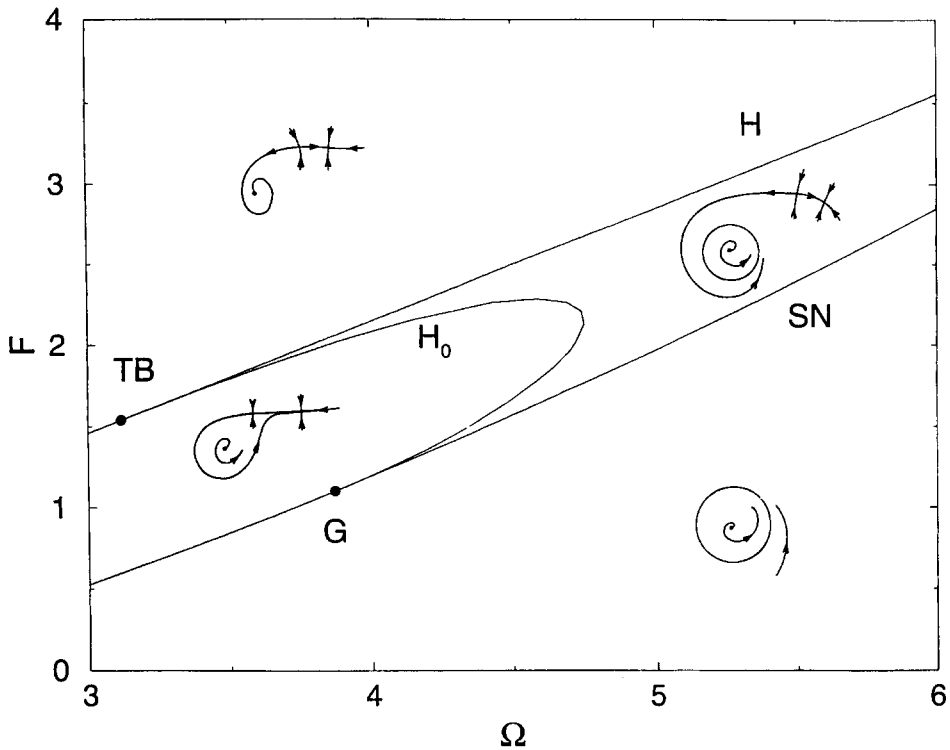

Fig. 5. Bifurcation diagram and phase portrait for Eq. (15) with $\alpha = 2$.

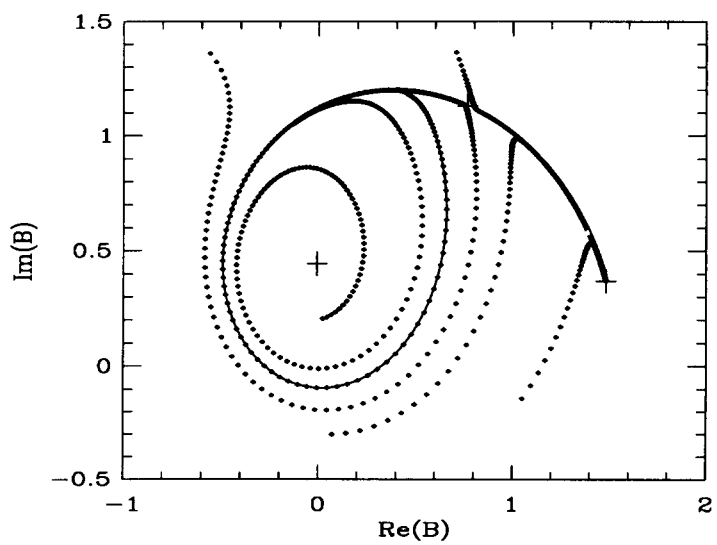

Fig. 6. Some trajectories for parameters ($\Omega = 5$, $F = 2.1$) in the centre-right region of the bifurcation diagram showing the attractive limit cycle (bold line), the stable fixed point and the two unstable fixed points (plus symbols).

with its inside unstable fixed point). The condition that Eq. (15) has a fixed point with a zero eigenvalue gives the equation of SN as

$$F_c^2 = \frac{2(1+\Omega\alpha)^3}{27(1+\alpha^2)^2}\left\{1+9\left(\frac{\Omega-\alpha}{1+\Omega\alpha}\right)^2-\left(1-3\left(\frac{\Omega-\alpha}{1+\Omega\alpha}\right)^2\right)^{3/2}\right\}. \tag{17}$$

On the contrary, when F is increased, the limit cycle shrinks around its inside fixed point and above the line H of Hopf bifurcations it is replaced by a stable fixed point. The condition that this fixed point has two purely imaginary opposite eigenvalues determines the equation of H as

$$8F^2 = 1+(\alpha-2\Omega)^2. \tag{18}$$

In addition to these local bifurcations, the centre-right region is also bounded by a line of global homoclinic bifurcations H_0 which has been determined numerically. When Ω is decreased the unstable fixed point outside the limit cycle moves toward the limit cycle, touches it and transforms it in a homoclinic orbit on H_0. To the left of H_0 the limit cycle does not exist anymore and only the three fixed points remain. On one side, the line H_0 ends on the line H of Hopf bifurcations at a Takens–Bogdanov bifurcation point TB at $\Omega = \alpha + 1/2\sqrt{1+\alpha^2}$. The other end is at the saddle-node bifurcation line SN at the codimension-two point G numerically determined as $\Omega = 3.87$, $F = 1.10$. The local bifurcation structure around such a point is analysed in [19]. Some supplementary bifurcation lines emanating from TB and G have not been plotted in Fig. 5.

Having determined the bifurcation set and the different phase portraits of Eq. (15), it can be seen where the operating point of the globally coupled system lies. In several cases that we have simulated, it lies very close to the saddle-node bifurcation line SN which separates a phase portrait with a stable fixed point and a stable limit cycle from one with only a limit cycle. For example, simulations at $\alpha = 2$, $\eta = -2$, $\mu = 2.2$ give a mean amplitude $\langle|\overline{A}|\rangle = 1.04$ and a peak frequency $\omega = -3.7$. Using Eq. (16), this gives $F = 1.77$, $\Omega = 4.75$ which is almost on the SN-line. The fluctuations of $\overline{A}$ in the globally coupled system make the system evolve between the two phase portraits and this qualitatively explains the ρ-shaped distribution of oscillators.

3.2. A one-parameter manifold of self-consistent states

Instead of taking the forcing parameters from the simulation data, one can try to determine them self-consistently. Namely, the imposed forcing (13) should agree with the forcing obtained by averaging the contribution of the different oscillators

$$R\exp(\mathrm{i}\omega t) = \frac{1}{N}\sum_{k=1}^{N} A_k. \tag{19}$$

Expressing this equality in terms of the B variable gives

$$R = \sqrt{\mu-1}\langle B\rangle\exp(\mathrm{i}\phi) \quad \text{or} \quad \langle B\rangle = \frac{\mu-1}{1+\eta^2}(1-\mathrm{i}\eta)F. \tag{20}$$

In (20), the average $(1/N)\sum_{k=1}^{N} B_j$ over the B_j has been replaced by the temporal average $\langle B\rangle$ of a single B solution of (15), assuming that the motions of the different oscillators are not correlated in the rotating frame. Eq. (20) is a complex equation so it gives two relations for the two unknown real parameters F and Ω, and it may seem to uniquely determine them (or at least to have a discrete number of solutions). In fact, this is only the case when the phase portrait consists of a single deterministic attractor. Otherwise, the proportions of oscillators on the

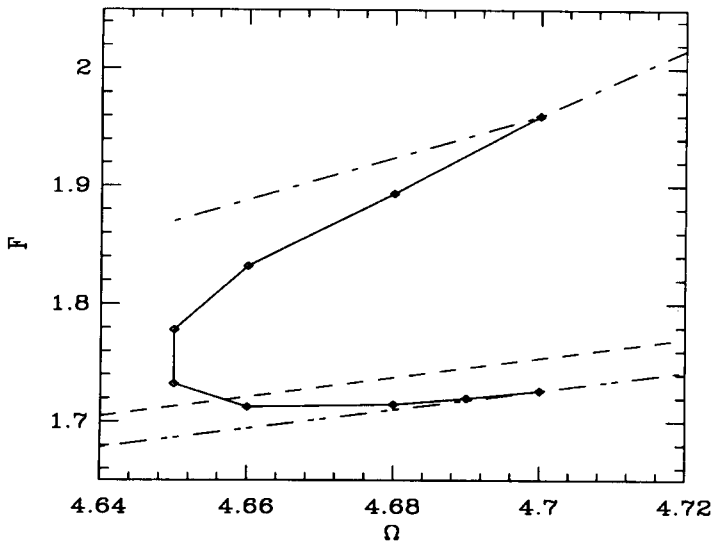

Fig. 7. Line of self-consistent solution(diamonds) for $\alpha = 2, \eta = -2, \mu = 2.2$. The line where the attractors shift dominance in the presence of a weak noise is also shown (dashed line) together with the saddle-node bifurction line (lower dot–dashed line) and the line of homoclinic bifurcations (upper dot–dashed line).

different stable deterministic attractors are additional free parameters (stability requirements lead to reject unstable attractors which could also contribute in principle) and a family of solutions depending on these free parameters is expected.

We have quantitatively analysed Eq. (20) for the same parameter choice as above ($\alpha = 2, \eta = -2, \mu = 2.2$). Below the line SN, the only stable attractor is the limit cycle and there are no additional parameters. In this region, we did not find any solutions of (20) other than the trivial solution $F = 0$. Above the line SN, there is both the stable limit cycle and a stable fixed point. Denoting by ρ the proportion of oscillators on the stable fixed point, Eq. (20) can be written as

$$\rho B_s + (1-\rho)\langle B\rangle_{lc} = \frac{\mu - 1}{1+\eta^2}(1 - i\eta)F, \tag{21}$$

where B_s is the position of the stable fixed point and $\langle B\rangle_{lc}$ is the time-averaged position on the limit cycle, and both are well-defined functions of F and Ω (and α). A solution of (21) was found for each ρ between 0.09 and, 0.16 (see Fig. 8). As shown in Figs. 7 and 8, this line $(\Omega(\rho), F(\rho))$ starts at $\rho = 0.09$ on the line H_0 of global homoclinic bifurcation and ends at $\rho = 0.14$ on the line SN of saddle-node bifurcations.

3.3. *Selection by an infinitesimal noise*

In the previous section, a family of self-consistent solutions has been found. We now argue that one of these solutions is privileged in the sense that it is the only one that is compatible with a weak noise in the forcing.

Let us suppose that Eq. (15) is perturbed by a weak noise that we assume to be gaussian for simplicity so that it is

$$\partial_\tau B = (1 + i\Omega)B - (1 + i\alpha)|B|^2 B + F + \eta(\tau) \tag{22}$$

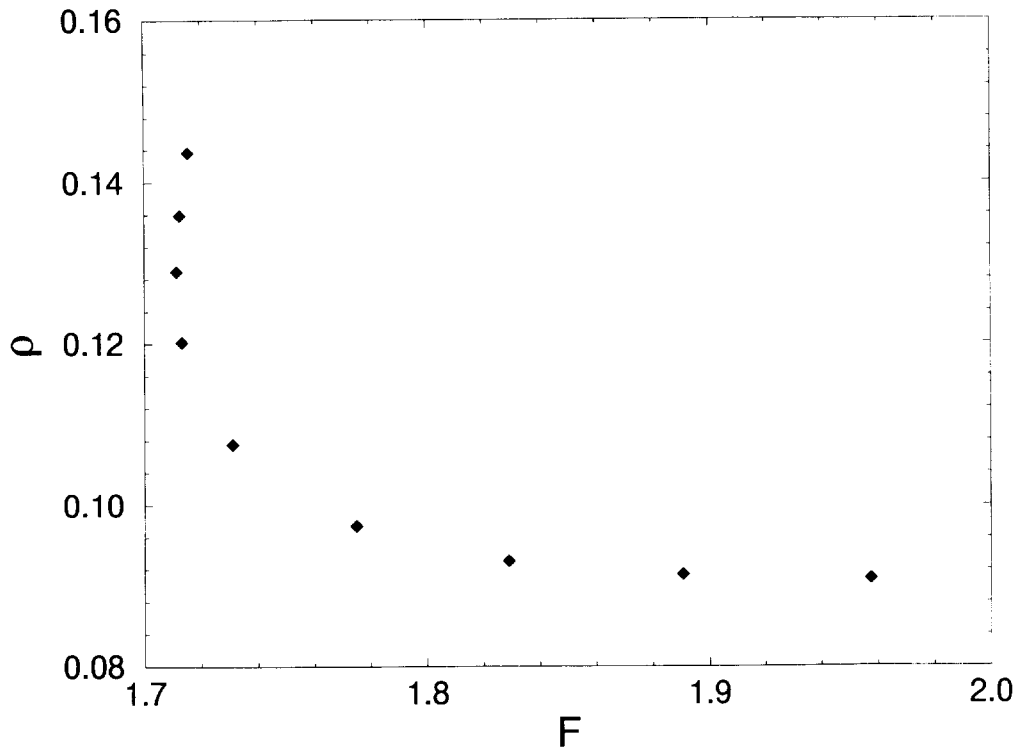

Fig. 8. Proportion of oscillators on the fixed point as one follows the line of self-consistent solutions ($\alpha = 2$, $\eta = -2$, $\mu = 2.2$).

with

$$\langle \eta(\tau)\eta^*(\tau')\rangle = 4D_\eta \delta(\tau - \tau'). \tag{23}$$

If F and Ω are chosen such that the deterministic equation admits as stable attractors a limit cycle and a fixed point, the oscillator will alternatively jump from one of these attractors to the other under the action of the noise. The noise amplitude will determine the fraction of time that the system spends on each of the two attractors. As we follow the line of self-consistent solutions $(\Omega(\rho), F(\rho))$, this noise determined proportion ρ_n will in general be different from the proportion ρ determined by the self-consistency condition. Only at particular points will the two coincide. It is easy to see that at least one such point should exist. The stable fixed point approaches the unstable fixed point and the barrier to escape from the fixed point vanishes near the SN-extremity of the self-consistency line. There, it certainly becomes smaller than the barrier to escape from the limit cycle . So, in a neighbourhood of the SN-extremity, the noise determined proportion of oscillators on the fixed point ρ_n is almost zero and therefore less than the self-consistently determined proportion $\rho = 0.14$. Near the H_0-extremity of the self-consistency line, exactly the opposite is true since the unstable fixed point approaches the limit cycle. Therefore ρ_n is almost 1 in a neighbourhood of the H_0-extremity and larger than $\rho = 0.09$ there. Continuity implies that there exists a point where ρ_n is equal to ρ.

We now proceed to the quantitative determination of this point. In the weak noise limit, for generic parameters, one attractor will exponentially dominate the other. The transition from $\rho_n = 1$ to $\rho_n = 0$ is very sharp and its position determines the crossing of the ρ_n and ρ curves on the self-consistency line. For a potential case, the population on each attractors would be given by Boltzmann weights and the transition would occur where the two attractors are

in potential wells of exactly the same depth. Here, however, a limit cycle and a fixed point are to be compared, so we need a generalization of this familiar result to the nonpotential case.

This interesting problem has been studied by a number of authors [9–12]. The answer is quite simple for a deterministic dynamical system perturbed by a weak gaussian noise:

$$\dot{\boldsymbol{x}} = \boldsymbol{F}(\boldsymbol{x}) + \boldsymbol{\eta}(t), \tag{24}$$

where $\boldsymbol{x}$ and $\boldsymbol{\eta}(t)$ are vectors in $\mathbb{R}^n$, and the noise η term is chosen such that

$$\langle \eta_i(t)\eta_j(t')\rangle = 2D\delta_{ij}\delta(t-t'). \tag{25}$$

In the weak noise limit ($D \ll 1$), what replaces the depth of the potential well for an attractor A is the minimum value $S(A)$ of $S(x) = \int_I |\dot{x} - F(x)|^2 \mathrm{d}t$ taken over all paths $x(t)$ which connect the attractor to the boundary of its basin of attraction. This result has been derived in two ways, either by considering the escape rate of the attractor A [9,11,12] (which behaves like $\exp(-S(A)/4D)$ for small D) or directly by considering the Fokker–Planck equation associated to (24) and estimating its solution in a WKB-like manner [10].

Varying $S(x)$, one obtains a system of $2n$ differential equations for the extremal path,

$$\dot{y}_j = -\sum_i \frac{\partial F_i}{\partial x_j} y_i, \qquad \dot{x} = F(x) + y(t) \tag{26}$$

with the boundary conditions that the path starts on the attractor A ($y(-\infty) = 0$, $x(-\infty) \in A$) and ends on the boundary of its basin of attraction (either at a finite or infinite time).

In our case, we have computed the escape integrals both for the limit cycle and for the stable fixed point, as explained in Appendix B. A typical result of this calculation is shown in Fig. 9 where the two escape integrals

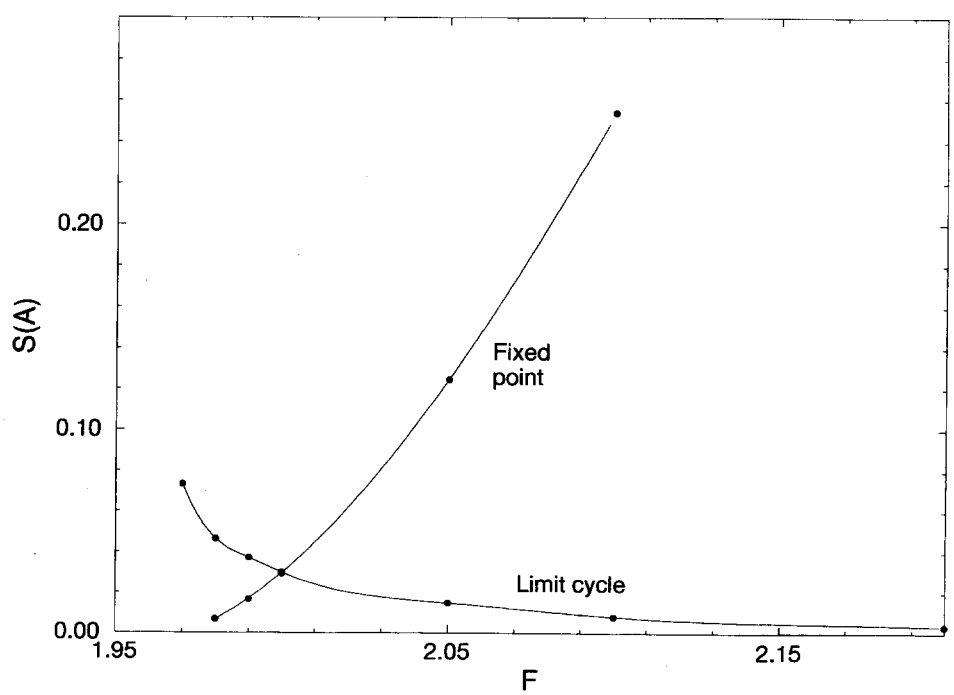

Fig. 9. Escape action for the fixed point and the limit cycle for $\Omega = 5$.

are plotted as a function of F, at fixed Ω. The crossing between the two curves is the value $F(\Omega)$ where the two attractors shift dominance in the weak noise limit. Namely, for $F < F(\Omega)$ almost all the oscillators are on the limit cycle (i.e. $\rho = 0$) and for $F > F(\Omega)$, almost all stay on the fixed point (i.e. $\rho = 1$).

The obtained curve $F(\Omega)$ is shown in Fig. 7. The point where it crosses the line of self-consistent solutions is the particular self-consistent solution that is selected by noise. It is in fair agreement with the results of direct simulation on the globally coupled system despite the fact that the escape actions are quite small and that fluctuations in $\overline{A}$ are sufficient to kick a significant number of oscillators out of the two deterministic attractors. The fact that the fixed point dominates over the limit cycle almost up to the saddle-node bifurcation line SN explains our earlier observation [7] that the parameters of the collective motion are quite close to SN. The effect of a small but finite noise is to push the self-consistent solution even much closer to SN as we show below.

4. Suppression of chaos in the collective dynamics by the addition of noise

In the previous section, we computed the characteristics of purely periodic regimes which we argued explain some characteristics of the regimes of region IV. The self-consistent periodic states are presumably unstable but some of their gross features are distinguishably recognizable in the more complex collective regimes of region IV, which are in some sense organized around them. We shall now see that by adding noise to the system (1), we can suppress chaos in the collective dynamics and stabilize the underlying periodic state [13]. We remark that the addition of noise has also been shown to increase the periodicity of the collective behaviour in other globally coupled systems [2,20].

We have simulated Eq. (1) with an added noise term,

$$\partial_t A_j = (1 + \mathrm{i}\eta)(\overline{A} - A_j) + \mu A_j - (1 + \mathrm{i}\alpha)|A_j|^2 A_j + \xi_j(t), \quad j = 1, \ldots, N, \tag{27}$$

where ξ_j is a complex white noise term with zero mean and variance D,

$$\langle \xi_j(t)\, \xi_{j'}^*(t') \rangle = 4D\delta(t - t')\delta_{jj'}. \tag{28}$$

Noise terms acting on different oscillators are uncorrelated.

Figs. 10 and 11 show the time series of $\mathrm{Re}(\overline{A}(t))$ and its power spectrum for $D = 0.01$. It is clearly seen that the time series of the collective motion is very regular in contrast to the deterministic case. The power spectrum is now very sharp and becomes sharper when the number of oscillators is increased. It is quite compatible with a purely periodic motion in the thermodynamic limit.

Nonetheless, the basic ρ-shape distribution of oscillators in the complex plane is still clearly recognizable as shown in Fig. 12. The effect cannot be simply attributed to a shift due to noise of the parameters of the deterministic system. In the deterministic case, there is no periodic regime with such a distribution of oscillators in the complex plane.

The characteristics of this noise-induced periodic behaviour can be obtained from the self-consistent approach described in the previous section but now, with a noise of finite amplitude D_η related to the amplitude of the stochastic term in Eq. (27) by $D_\eta = D/(\mu - 1)^2$.

In the presence of noise, there is a well-defined invariant measure, and the self-consistent equation (20) has a unique solution for each noise amplitude. The corresponding amplitude $|\overline{A}(D)|$ of the periodic motion is shown in Fig. 13. It predicts a first-order transition to $\overline{A} = 0$ for $D \simeq 3.8 \times 10^{-2}$ (which, of course, strictly only exists in the thermodynamic limit of an infinite number of oscillators). This is confirmed by simulations with increasing numbers of oscillators as shown in Fig. 13. It can also be noted that even a quite small noise amplitude shifts significantly the average amplitude of the individual oscillator away from the zero-noise limit value.

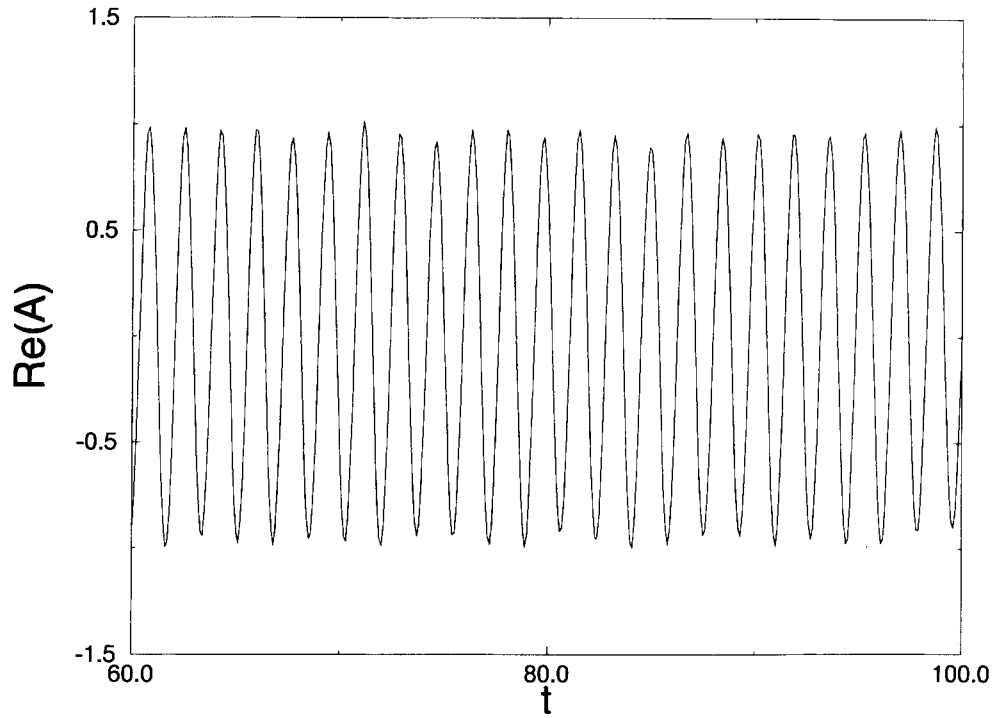

Fig. 10. Time series of $\overline{A}(t)$ with noise ($D = 0.01$). Other parameters are as in Fig. 1.

For the parameter values of Figs. 10–13, it is difficult to numerically quantify the lower noise threshold corresponding to the transition from a chaotic collective motion to a periodic one. One possibility could be that it corresponds to the noise level needed to push the self-consistent solution below the SN line (see Fig. 7). Another possibility is that the periodic self-consistent solution is unstable in the globally coupled system because the oscillators on the limit cycle tend to synchronize. A desynchronization transition at a finite noise level as analysed in [1] would then stabilize the periodic self-consistent solution.

5. Conclusions

We have analysed the dynamics of the globally coupled system of oscillators (1). As in other such systems, a variety of dynamical regimes has been found. We have particularly stressed the existence of complex collective regimes which exist even when the number of oscillators becomes large. We have noted that precise tools are lacking to fully analyse the collective dynamics in the thermodynamic limit. Understanding some of its main characteristics using a simple self-consistent approach has directly led us to consider and compute the nonequilibrium generalization of usual Boltzmann weights. Finally, we have shown that adding noise has a regularizing influence on the collective dynamics, as already noted in other cases. It remains to be seen whether this will have some interesting applications.

Appendix A. Linear stability of regimes I and II

We summarize here our computation of the stability of the simple periodic states of regimes I and II.

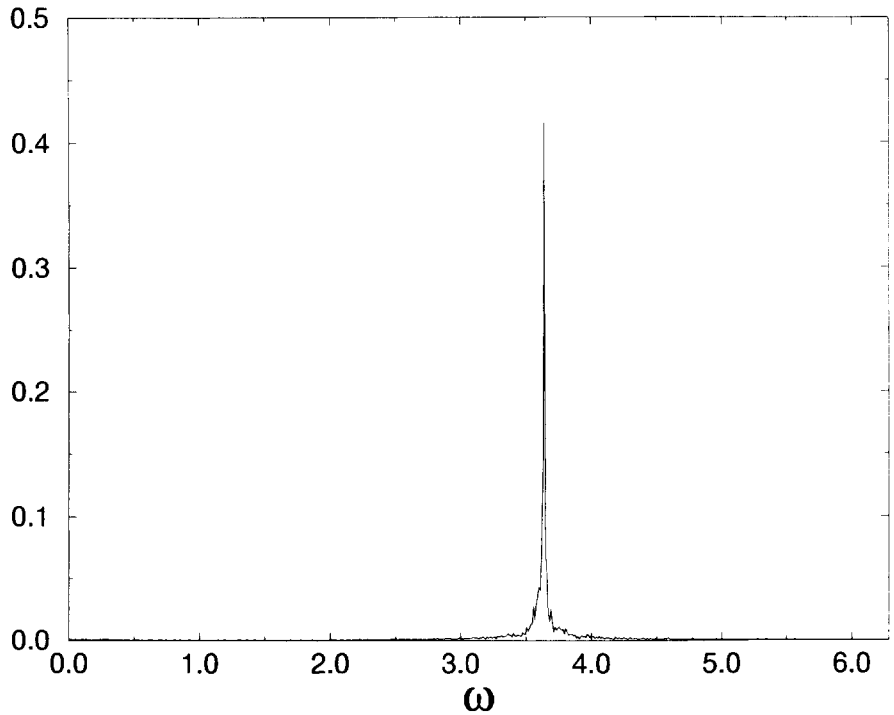

Fig. 11. Power spectrum of $\mathrm{Re}(\overline{A}(t))$ with noise ($D = 0.01$). Other parameters are as in Fig. 2.

In regime I, all oscillators are identical to $\overline{A} = \sqrt{\mu}\exp(-\mathrm{i}\alpha\mu t)$. Eq. (1) is linearized by substituting A_j under the form

$$A_j(t) = (\sqrt{\mu} + a_j)\exp(-\mathrm{i}\alpha\mu t). \tag{A.1}$$

The linear evolution of the perturbation a_j is obtained as

$$\frac{\mathrm{d}a_j}{\mathrm{d}t} = \frac{1+\mathrm{i}\eta}{N}\sum_k a_k - (1+\mathrm{i}\eta)a_j - \mu(1+\mathrm{i}\alpha)(a_j + a_j^*) \tag{A.2}$$

(here and below the * denotes complex conjugation). In the $(2N-2)$ real vector space where $\sum_k a_k = 0$ one obtains $(N-1)$ times the couple of eigenvalues (λ_1, λ_2) of the 2×2 matrix

$$\begin{pmatrix} -1-2\mu & \eta \\ -\eta - 2\mu\alpha & -1 \end{pmatrix}, \tag{A.3}$$

(λ_1, λ_2) are therefore the roots of the characteristic polynomial given in Eq. (6) of the main text. In addition to these $(2N-2)$ eigenvalues, there are two eigenvalues obtained by diagonalizing the system (A.2) in the two-dimensional space where all a_j are equal. This gives the equation

$$\frac{\mathrm{d}a}{\mathrm{d}t} = -\mu(1+\mathrm{i}\alpha)(a + a^*). \tag{A.4}$$

The remaining two eigenvalues are therefore equal to 0 and -2μ.

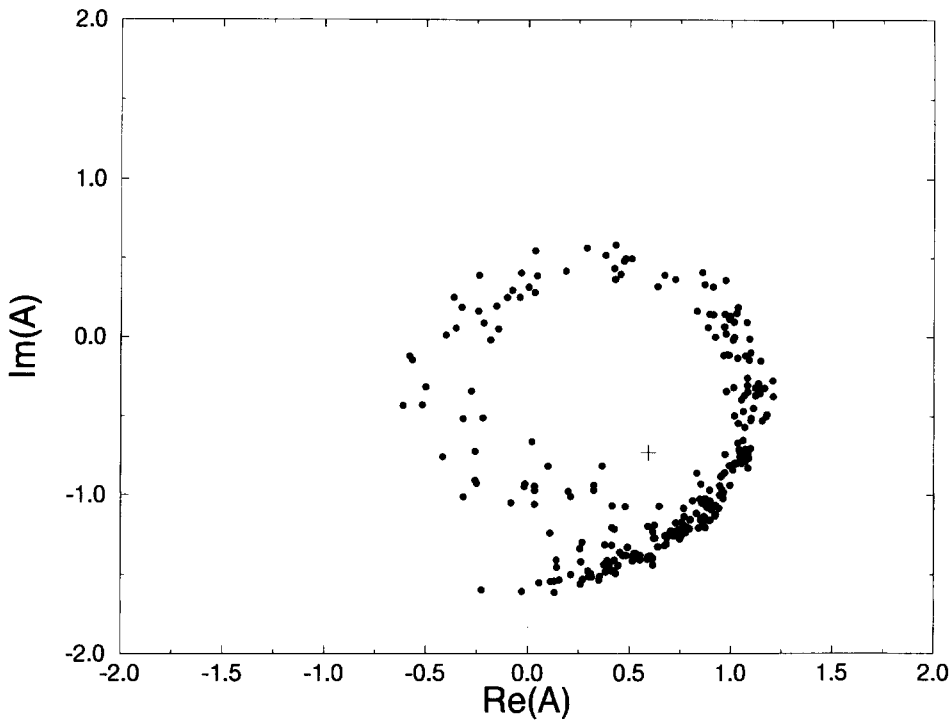

Fig. 12. Distribution of oscillators with noise ($D = 0.01$). The ρ-shape is still clearly visible. Other parameters are as in Fig. 2.

The stability analysis of the states of regimes II is very similar. A perturbation to one of these states is written in the form

$$A_j = (\sqrt{\mu - 1} + a_j)\,\exp(\mathrm{i}[(\alpha - \eta - \alpha\mu)t + \phi_j]). \tag{A.5}$$

After linearization, the equation for the perturbation a_j is obtained as

$$\frac{\mathrm{d}a_j}{\mathrm{d}t} = \frac{1 + \mathrm{i}\eta}{N} \sum_k a_k \exp \mathrm{i}(\phi_k - \phi_j) - (\mu - 1)(1 + \mathrm{i}\alpha)(a_j + a_j^*). \tag{A.6}$$

It is useful to note that both the global coupling and the whole operator on the RHS of (A.6) leave invariant the four-dimensional subspace S_4 spanned by the four vectors $\{a_j^{(1)} = \cos(\phi_j),\ a_j^{(2)} = \sin(\phi_j),\ a_j^{(3)} = \mathrm{i}\cos(\phi_j),\ a_j^{(4)} = i\sin(\phi_j)\}$ and its orthogonal. In the subspace orthogonal to S_4, the global coupling vanishes and one obtains the system

$$\frac{\mathrm{d}a_j}{\mathrm{d}t} = -(\mu - 1)(1 + \mathrm{i}\alpha)(a_j + a_j^*)a. \tag{A.7}$$

This gives $N - 2$ eigenvalues zero for eigenvectors of the form $a_j = \mathrm{i}x_j$ with the two orthogonality constraints $\sum_j x_j \cos(\phi_j) = 0$, $\sum_j x_j \sin(\phi_j) = 0$ and $N - 2$ eigenvalues $-2(\mu - 1)$ for $a_j = (1 + \mathrm{i}\alpha)y_j$ with the same orthogonality constraints on the y_j. It remains to diagonalize (A.6) in S_4. This is conveniently done in complex coordinates by writing $a_j = a\exp(-\mathrm{i}\phi_j) + b\exp(\mathrm{i}\phi_j)$. The time evolution of (a, b^*, b, a^*) is given by the 4×4 matrix

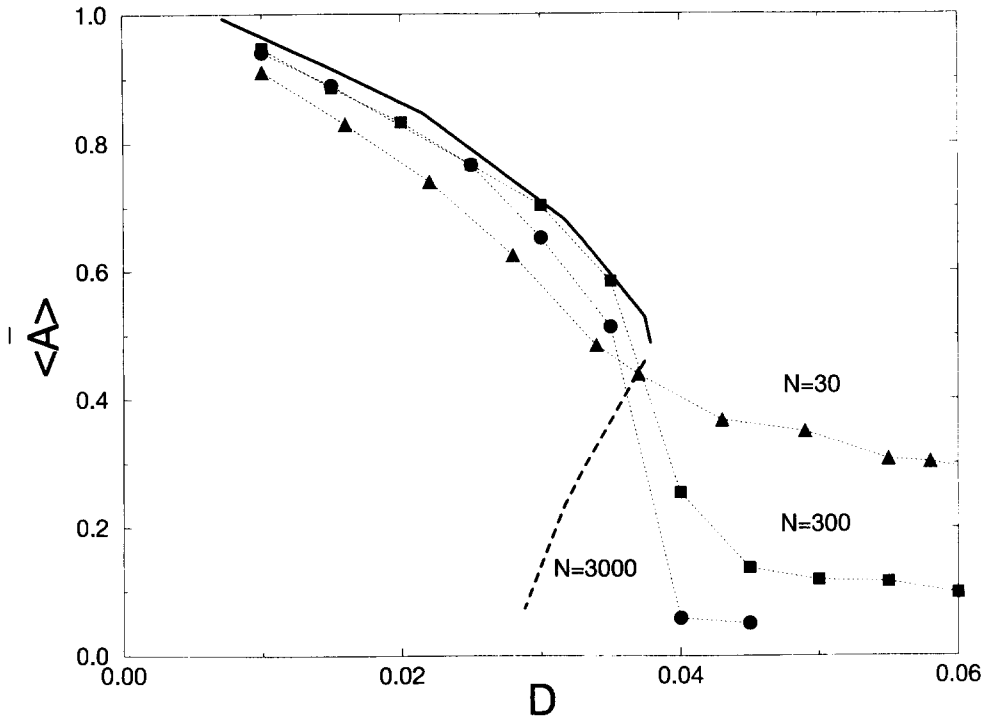

Fig. 13. Amplitude of the collective motion as a function of the noise level for different numbers of oscillators. Other parameters are as in Fig. 2. The curve obtained by solving the self-consistent equation (20) and the relations (16) is shown for comparison as a bold line (the dashed part corresponds to unstable solutions).

$$\begin{pmatrix} u & v & w & 0 \\ v^* & v^* & 0 & 0 \\ 0 & 0 & v & v \\ 0 & w^* & v^* & u^* \end{pmatrix}, \tag{A.8}$$

where $u = 1+i\eta-(\mu-1)(1+i\alpha)$, $v = -(\mu-1)(1+i\alpha)$. $w = (1+i\eta)\delta$ depends on the particular state considered but only through the parameter $\delta = 1/N \sum_k \exp(2i\phi_k)$. If $|\delta| \equiv \Delta = 0$, the matrix (A.8) is block diagonal and the four eigenvalues are the roots of its characteristic polynomial given as $P_2(\lambda)P_2^*(\lambda)$ with

$$P_2(\lambda) = \lambda^2 + b\lambda + c. \tag{A.9}$$

The complex coefficients $b = b_1 + ib_2$ and $c = c_1 + ic_2$ are given by

$$b = 2\mu - 3 - i\eta, \qquad c = (1-\mu)(1+i\eta)(1-i\alpha). \tag{A.10}$$

For general Δ, one obtains the characteristic polynomial $P_4(\lambda)$ of Eq. (8),

$$P_4(\lambda) = P_2(\lambda)P_2^*(\lambda) - d \tag{A.11}$$

with

$$d = \Delta^2(\mu-1)^2(1+\alpha^2)(1+\eta^2). \tag{A.12}$$

For $\Delta = 0$, the roots can be explicitly computed and a simple computation gives the stability criterion as

$$\mathrm{Re}(b) = b_1 > 0, \qquad b_1^2 c_1 + b_1 b_2 c_2 - c_2^2 > 0. \tag{A.13}$$

Using (A.10), this gives the stability condition (10) of the main text. For general Δ, one can apply the Routh–Hurwitz criterion to $P_4(\lambda)$. This directly gives the stability criterion

$$\mathrm{Re}(b) = b_1 > 0, \qquad |b|^2(b_1^2 c_1 + b_1 b_2 c_2 - c_2^2) + d b_1^2 > 0, \tag{A.14}$$

which is equivalent to (11) of the main text using (A.10) and (A.12). Moreover, since d is positive, it is clear that (A.14) is weaker than (A.13) and that states with unevenly distributed phases have a larger domain of stability than the state with uniformly distributed phases. This completes the stability of (1) around states of regimes I and II.

Appendix B. Computation of escape paths and actions

We consider Eq. (22) with F and Ω in the centre-right region of Fig. 5 so that the deterministic equation has both a stable limit cycle and a fixed point. For weak noise, the system spends exponentially different proportions of its time in the neighbourhood of each attractor. As recalled in Section 3.3, one has to compare the escape actions for the two attractors. In the specific case of Eq. (22), one should minimize the action

$$\int_{t_{\min}}^{t_{\max}} \mathrm{d}\tau \| \partial_\tau B - (1 + \mathrm{i}\Omega) B + (1 + \mathrm{i}\alpha)|B|^2 B - F \|^2 \tag{B.1}$$

along a path going from the attractor to the boundary of its basin of attraction. The deterministic motion does not contribute anything to (B.1). Therefore, for any path, it is always possible to take the lower time limit of the integral as $-\infty$ without changing the integral (B.1), by adding, if necessary, a deterministic motion on the attractor from $t = -\infty$ to $t = t_{\min}$. Similarly, the boundary of the attractor basin of attractions is formed by the stable manifold of the unstable fixed point. So, it is possible to take the upper time limit in (B.1) as $+\infty$ and the end point of the path as the unstable fixed point (again adding if necessary a deterministic motion to the unstable fixed point along its stable manifold from $t = t_{\max}$ to $t = +\infty$). Moreover, a local analysis shows that a nonsmooth path cannot be a local minimum of (B.1). So, the smooth optimal path starts from the attractor at $t = -\infty$ and ends on the unstable fixed point at $t = +\infty$. [1]

Varying (B.1), one obtains the equations obeyed by this optimal path,

$$\begin{aligned} \partial_\tau B &= (1 + \mathrm{i}\Omega) B - (1 + \mathrm{i}\alpha)|B|^2 B + F + C, \\ \partial_\tau C &= -(1 - \mathrm{i}\Omega) C + 2(1 - \mathrm{i}\alpha)|B|^2 C + (1 + \mathrm{i}\alpha) B^2 C^*. \end{aligned} \tag{B.2}$$

As stated, the boundary conditions are

$$B(-\infty) \in A, \quad C(-\infty) = 0 \quad \text{and} \quad B(+\infty) = B_{\mathrm{u}}, \quad C(+\infty) = 0, \tag{B.3}$$

[1] In [12], it is found in a similar situation that the optimal path from the limit cycle reaches the unstable fixed point in a finite time. We believe it is a numerical artifact. It is equivalent to determine an optimal escape path or an optimal path joining the limit cycle to the stable fixed point since once the path has reached the boundary of the limit cycle basin of attraction it follows a deterministic trajectory to reach the stable fixed point (since a deterministic motion does not contribute to the action integral). Again this optimal path cannot be discontinuous and the optimal escape path cannot reach the unstable fixed point with a finite "noise" coordinate.

where A is one of the deterministic attractors (the limit cycle or the fixed point B_s) and B_u is the unstable fixed point. In the potential case, such an optimal path can be simply obtained by reversing the classical deterministic trajectory going from the unstable fixed point to the stable attractor. This is not the case here and the optimal paths and their associated actions have to be found numerically. In both cases, they were obtained by a shooting method.

Linearization of the system (B.2) around the stable fixed point (B_s, $C = 0$) gives two negative eigenvalues (those of the deterministic system) and two opposite positive eigenvalues. The path should reach (B_s, $C = 0$) at $t = -\infty$. So, it should belong to the two-dimensional unstable manifold of this point which coincide in the neighbourhood of (B_s, $C = 0$) with its tangent subspace spanned by the two positive eigenvectors. In principle a simple one-parameter shooting strategy is applicable. One chooses a small circle around the origin of the two-dimensional vector space and computes the outgoing trajectory for a given angle. The starting angle is then adjusted so that the projection of the trajectory on the B coordinates reaches the unstable fixed point B_u. In practice, a difficulty arises from the fact that close to the saddle-node bifurcation, one of the positive eigenvalue tends to zero and thus becomes much smaller than the other. This greatly magnifies the component of the trajectory in the direction of the dominant eigenvector so that a very small starting component in this direction should be chosen. Numerical precision becomes the limiting factor. For a starting point close to (B_s, $C = 0$), the finite magnitude of the smallest computer number is dramatically amplified and all the computable trajectories are found to pass at a finite distance from the unstable fixed point. This problem was handled by choosing the numerical trajectory endpoints at small finite distances of both (B_s, $C = 0$) and (B_u, $C = 0$). The remaining parts of the trajectory were analytically obtained by the linearization of (B.2) in the neighbourhood of these fixed points. It was of course checked that changing the distances did not significantly change the results.

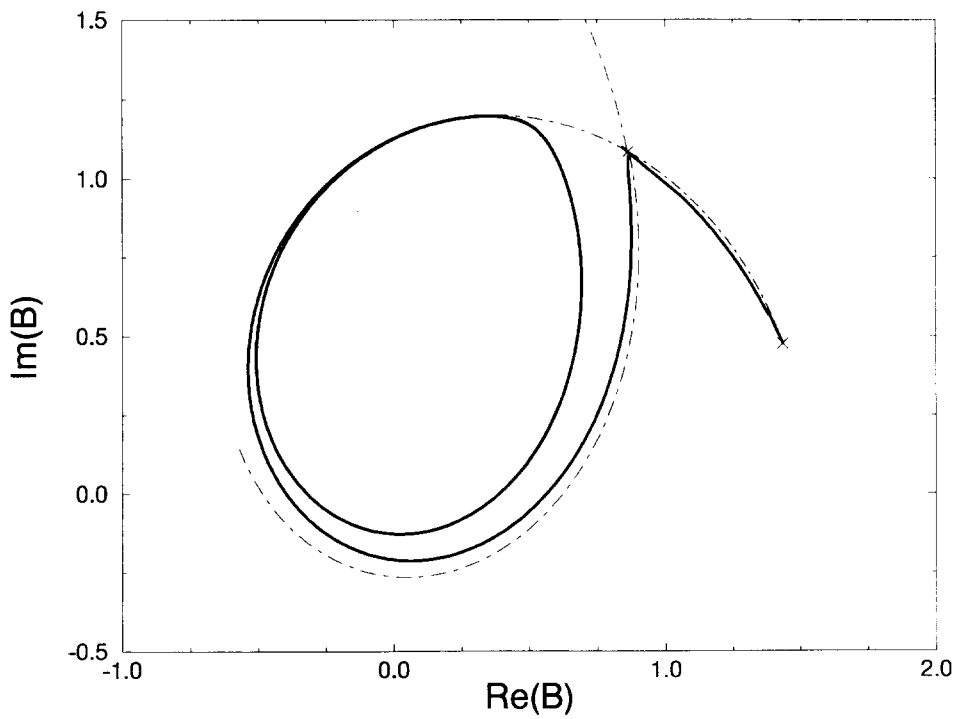

Fig. 14. The computed optimal escape trajectories from the stable fixed point and the stable limit cycle (thick bold lines) for $\Omega = 5$, $F = 2.05$. The stable and unstable manifold of the unstable exit fixed point are also shown.

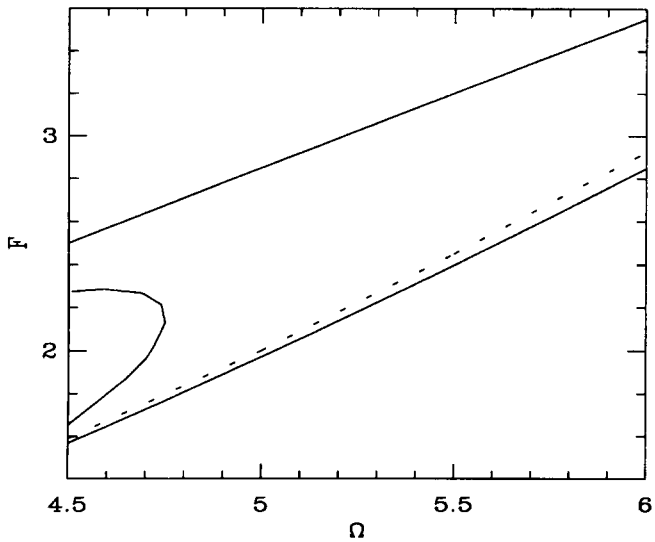

Fig. 15. The line where the escape actions of the stable fixed point and the limit cycle are equal (dashed). The main bifurcation lines are also shown.

Obtaining the optimal path starting from the limit cycle and reaching the unstable fixed point turned out to be technically simpler. Linearization of the system (B.2) around the deterministic limit cycle (with $C = 0$) gives one negative and one zero Lyapounov exponents and their two opposites. So, at a given point around the limit cycle there is only one expanding direction. The coordinate along this direction parametrizes the different outgoing paths and can be used as a shooting parameter to find the optimal one (the one which reaches (B_u)). In practice, this was done as in [12]. A point B on the limit cycle was obtained by iterating the deterministic system . It was taken as the starting point together with a very small imaginary C (less than 10^{-4}) used as the shooting parameter.

The two obtained optimal paths for $\Omega = 5$, $F = 2.05$ are shown in Fig. 14. The corresponding actions are $S = 1.4 \times 10^{-2}$ for the limit cycle and $S = 0.12$ for the fixed point. By varying F, the point $F(\Omega)$ where the two escape actions are equal is determined as shown in Fig. 9. By repeating this procedure, one obtains the curve $F(\Omega)$ shown in Figs. 7 and 15.

References

[1] Y. Kuramoto, Chemical Oscillators, Waves and Turbulence (Springer, New York, 1984).
[2] K. Kaneko, Phys. Rev. Lett. 63 (1989) 219; Phys. Rev. Lett. 65 (1990) 1391; Physica D 55 (1992) 368 and references therein.
[3] Y. Kuramoto and Y. Nishikawa, J. Statist. Phys. 49 (1987) 569; H. Daido, Phys. Rev. Lett. 68 (1992) 1073.
[4] K. Wiesenfeld and P. Hadley, Phys. Rev. Lett. 62 (1989) 1335.
[5] P.C. Matthews, R.E. Mirollo and S.H. Strogatz, Physica D 52 (1991) 293.
[6] D. Golomb, D. Hansel, B. Shraiman and H. Sompolinsky, Phys. Rev. A 45 (1992) 3516.
[7] V. Hakim and W.-J. Rappel, Phys. Rev. A 46 (1992) R7347.
[8] N. Nakagawa and Y. Kuramoto, Progr. Theoret. Phys. 89 (1993) 313; Physica D 75 (1994) 74.
[9] M.I. Freidlin and A.D. Wentzell, Random Perturbations of Dynamical Systems (Springer, New York, 1984).
[10] R. Graham and T. Tél, Phys. Rev. A 31 (1985) 1109; Phys. Rev. A 33 (1986) 1322.
[11] R.L. Kautz, Phys. Rev. A 38 (1988) 2066.
[12] P. Grassberger, J. Phys. A 22 (1989) 3283.
[13] V. Hakim and W.-J. Rappel, Europhys. Lett. 27 (1994) 637.
[14] T.B. Benjamin and J.E. Feir, J. Fluid Mech. 27 (1967) 417; A.C. Newell, Lectures in Appl. Math. 15 (1974) 157; J.T. Stuart and R.C. DiPrima, Proc. Roy. Soc. (London) A 362 (1978) 27.

[15] F. Gantmacher, Matrix Theory, Vol. II (Chelsea, New York) p. 173.
[16] N. Nakagawa and Y. Kuramoto, Physica D 80 (1995) 307.
[17] F. Takens, Lecture Notes in Math. 288 (1981) 366.
[18] J.M. Gambaudo, J. Diff. Equations 57 (1985) 172–199; P. Glendinning and MRE Proctor, to be published; and references therein.
[19] S. Schecter, SIAM J. Math. Anal. 18 (1987) 1142.
[20] G. Perez and H.A. Cerdeira, Phys. Rev. A 46 (1992) 7492.